This is the accepted manuscript made available via CHORUS. The article has been published as:

Infinite-stage Nernst-Ettingshausen Cryocooler for Practical Applications

M. Mobarak Hossain Polash and Daryoosh Vashaee

Phys. Rev. Applied **15**, 014011 — Published 8 January 2021

DOI: 10.1103/PhysRevApplied.15.014011

Infinite Stage Nernst-Ettingshausen Cryocooler for Practical Applications

Md Mobarak Hossain Polash[1,2] and Daryoosh Vashaee[1,2*]

[1]Department of Materials Science and Engineering, North Carolina State University, NC 27606 USA
[2]Department of Electrical and Computer Engineering, North Carolina State University, NC 27606 USA

Abstract: Recent developments in Nernst-Ettingshausen (NE) physical phenomena combined with advances in the performance of rare-earth permanent magnets makes thermomagnetic (TM) cryocoolers well suited for practical applications. The device performance of a NE cryocooler depends on both the material and the geometrical shape of the device. Despite the continued progress in TM materials, the optimum shape is still based on a simplified infinite-stage model derived by T. C. Harman in 1963 [1]. Harman's model assumes several non-realistic assumptions, such as temperature-independent material properties and constant current density. We are relaxing such assumptions and derive a fully temperature-dependent numerical model to accurately solve for the thermomagnetic features of a Nernst-Ettingshausen cooler (NEC) with arbitrary geometry. We correct Harman's analytical function and compare its performance with various shaped devices. The corrected shape has a higher Coefficient of Performance (COP) at higher temperature differentials, which indicates that when the material resistivity is a strong function of the temperature, the corrected infinite stage device can provide better performance than Harman's geometry. Moreover, the corrected shaped device can provide higher heat flow density at a similar optimum COP condition. A case study based on the state-of-the-art TM material, BiSb alloy, is presented, and the critical parameters for designing an efficient thermomagnetic cooler are discussed in detail.

Key Words: Infinite stage, Nernst-Ettingshausen, Thermomagnetic, Cryogenic cooler, BiSb

Introduction

Solid-state coolers such as Thermoelectrics (TE) based on the Peltier-Seebeck effect and Thermomagnetics based on the Nernst-Ettingshausen effect have taken much attention as competitive green technologies for next-generation cooling applications over the conventional methods due to their near-zero Ozone depletion potential and global warming potential [2-5]. Moreover, these devices offer many salient features like a long lifetime, high reliability, no moving parts, low maintenance cost, flexible form-factor, small size, efficient localized cooling, light-weight, fast and dynamic response, better thermal control, noise- and vibration-free application, which helps to improve the resolution of cooled infrared focal-plane arrays, no refrigerants, and cost competitiveness [6,7]. Solid-state coolers are linearly coupled systems governed by Onsager's theorem, where the entropy is carried by charge, heat, and spin carriers (spin or spin-wave) of the system in the presence or absence of a magnetic field via diffusive and advective transport process [8-11]. Each type of solid-state cooler has its own efficient operating temperature range [7,12]. Among them, thermomagnetic (TM) devices show better performance at the cryogenic temperature range (< 200K) [7,12]. Compared to Peltier or TE coolers (TEC), TM or NE coolers (NEC) provide higher temperature differentials at the cryogenic temperature

*Corresponding author email: dvashae@ncsu.edu

range, which can be further increased by cascading. TE or Peltier coolers can achieve a large temperature differential with multistage cascading, which is practically limited to 5-6 stages [12]. Moreover, NECs have smaller losses due to lower contact resistance compare to TECs. The device performance of NE cryocoolers depends on both the shape of the device and the material properties under the transverse magnetic field [7,12]. Recent findings of exotic thermomagnetic effects in different materials [13-16] show huge prospects in enhancing thermomagnetic performance from a material perspective, which has revived the research on NE cryocoolers. However, fewer works [7,17-19] addressed the contribution of the geometric shape of NE devices to enhance its performance. Till now, the infinite-stage shape, derived by T. C. Harman in 1963 [1], has been considered the most optimum shape for the cascade structure. Harman's model is based on some idealistic assumptions of temperature-independent material properties and, therefore, temperature independent current density. This assumption introduced an excess Joule heating, and therefore, there is a possibility to optimize the infinite-stage shape further by utilizing more realistic considerations.

Infinite-stage cascading can enhance the performance of the NECs by increasing the cross-sectional area in the direction of the heat flow, which improves the heat pumping capacity of the successive stages [20]. Infinite-stage cascading is not possible for TE devices. But an infinite-staged NEC can be built from a single block of material, as there is no need for electrical isolation between the stages [20]. The need for permanent magnets may make these devices bulky and costly. However, with the invention of the strong rare earth magnets, magnetic fields as high as 0.6 T are accessible with reasonable size magnets [21,22]. In general, solid-state coolers suffer from low-efficiency due to low figure-of-the merit (zT) resulted from the counter-indicative properties that define the zT, such as electrical conductivity, thermal conductivity, Seebeck coefficient, or Nernst coefficient [7,12,23-24]. In NE devices, zT has a $T^{7/2}$ dependence; hence, it drops more quickly with lowering the temperature [25]. Low zT reduces the efficiency of the solid-state cooler below that of the vapor compression-based coolers [6,7]. Several TE and TM devices were found promising for cryogenic applications [26-29], yet more research is needed to improve the performance of these devices further to meet the application needs.

Recent research on solid-state coolers is mostly focused on discovering TE materials with high zTs [30,31]. Compared to TEs, less research has been conducted on TM materials and devices [32-35]. But the recent resurgence of the need for solid-state cryocoolers has triggered the need for improving the material properties as well as optimizing the device structure. Till now, most of the works [36-38] on NE device shape were based on Harman's exponential shape, ignoring the conceptual approximations in deriving the exponential infinite-stage shape [7,37]. This work will address some limitations of prior works, such as constant current density and resistivity approximations [1,37]. We develop a corrected version of Harman's shaping function, considering a variable current density for a constant electric field and temperature-dependent electrical resistivity. A comprehensive comparison of the device parameters is derived in terms of the maximum heat pump density, Coefficient of Performance (COP), and transverse temperature gradient among different shaped devices, including rectangular, trapezoid, Harman's infinite shape, and the corrected infinite geometry. The degree of enhancement among different geometries determines the right shape for a target application as the construction of the infinite

state device can be costly; hence, it is not always the best solution. We will further introduce a numerical engine that can calculate the different device properties considering the realistic temperature dependence of the material properties for an arbitrary shape cooler. The numerical model is applied to calculate the properties of several coolers with different shapes based on the well-known BiSb alloy for TM applications [38,39]. According to the numerical analysis, the corrected geometry has the highest COP when the current density and heat flow are at their optimum values. However, in practice, one may desire to increase the cooling power or the heat flow at the cost of lower COP. Under such conditions, trapezoid geometry can deliver higher heat flow at reasonable COP, which is also a more accessible geometry for fabrication.

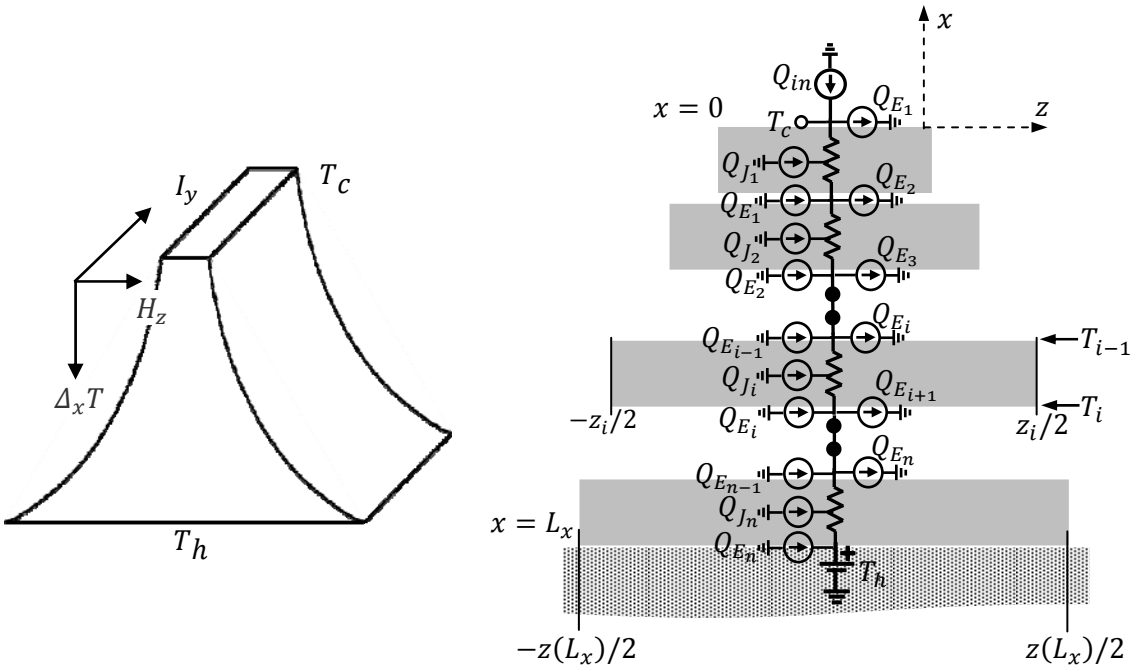

Figure 1: (Left) Infinite staged Nernst-Ettingshausen (NE) device along with the direction of the magnetic field, current flow, and temperature gradient, and (Right) representation of an infinite staged device with single staged parallelepiped NE elements along with corresponding equivalent circuit model.

Derivation of the Corrected Infinite Staging Function

The formalism of the corrected infinite staging function was obtained by following similar steps as Harman's method, however, with no limiting assumption on the current density. It is convenient to consider the infinite staged device as a combination of many single stages with parallelepiped geometry, as shown in Figure 1. In a multistage device, each stage pumps the combination of heat from the previous stage and the joule heating of the present stage to the next stage [7,20]. Therefore, the following stages must be able to pump more heat, which requires the size of the single staged element to increase in the heat flow direction. The general assumptions to derive the size and shape of the successive stages are the energy conservation principle and optimum coefficient of performance (COP) among the stages [1]. It is mention-worthy that maximum COP (COP_{Qmax}) and optimum COP (COP_{opt}) in NE devices have different definitions. Maximum COP (COP_{Qmax}) is associated with the maximum cooling power, Q_{max}. Therefore,

COP_{Qmax} is not necessarily the highest COP of a NE device. Instead, optimum COP (COP_{opt}) is associated with the highest COP condition of the device. At optimum COP, the device operates at an economical current but with a lower heat flow rate. Therefore, the cooling power may fall too small to provide any useful cooling, which may not be desired for many applications.
Following Harman's derivation technique (see appendix for more details), the primary differential relation among power (P), rate of heat flow ($\dot{\epsilon}$), and temperature (T) can be expressed as [1]:

$$\frac{dP}{P} = \frac{d\dot{\epsilon}}{\dot{\epsilon}} = \frac{dT}{TF^i(\delta)} \qquad (1)$$

Here, $F(\delta)$ is derived from the COP of a single-stage rectangular device as [1,40]:

$$COP = \frac{T_0}{\Delta_x T}\frac{(1-\delta\frac{T_L}{T_0})}{(1+\delta)} = C(T)F(\delta) \qquad (2)$$

where $C(T)$ denotes the Carnot efficiency of the device and $F(\delta)$ is a function of δ where $\delta = (1 - z_{NE}\bar{T})^{1/2}$. z_{NE} is the thermomagnetic figure-of-merit expressed as [20]

$$z_{NE} = \frac{(\alpha_{yx} + H_z N_{yx})^2}{\kappa_{xx}\rho_{yy}} \qquad (3)$$

where α_{yx} is the magneto-Seebeck coefficient along the yx plane (a negligible term that often ignored in literature), H_z is the magnetic field in the z-direction, N_{yx} is the Nernst coefficient in the yx plane, κ_{xx} is the thermal conductivity in the x-direction, and ρ_{yy} is the electrical resistivity in the y-direction.

It is worth clarifying four different types of figure-of-merit (z_{NE}) found in the literature [37,41]. The differences are for the isothermal or adiabatic material properties. The first definition is $z_{NE} = (H_z N_{yx})^2/\rho_{yy}\kappa_{xx}$, where the material properties are isothermal and $0 \le z_{NE} \le 1$. The second definition is $z_{NE}{}^* = (H_z N_{yx})^2/\rho_{yy}\kappa_{xx}{}^* = z_{NE}/(1 + z_{NE}T)$ where $\kappa_{xx}{}^* \equiv \kappa_{xx}(1 + z_{NE}T)$, and always $z_{NE}{}^*T < 1$. In most experiments, one measure $\kappa_{xx}{}^*$ because there is usually no load connected to the sample, hence, $J_{yy} = 0$ and $\kappa_{xx}{}^*$ includes transverse corrections due to the Nernst effect on electrical conductivity and the Ettingshausen effects [41]. The third definition is the adiabatic Ettingshausen figure-of-merit that assumes adiabatic resistivity, i.e. $\rho^a_{yy} = \rho_{yy}/(1 + z_{NE}T)$ and hence, $z^a_{NE} = (H_z N_{yx})^2/\rho^a_{yy}\kappa_{xx}$. z^a_{NE} can take any value from zero to infinity. Finally, forth Ettingshausen figure-of-merit considers ρ^a_{yy} and $\kappa_{xx}{}^*$. Therefore, the forth figure-of-merit is $z^{a*}_{NE} = (H_z N_{yx})^2/\rho^a_{yy}\kappa_{xx}{}^*$. Since $\rho^a_{yy}\kappa_{xx}{}^* = \rho_{yy}\kappa_{xx}$, we have $z^{a*}_{NE} = z_{NE}$. Due to the existence of different definitions of z_{NE}, it is vital to understand which z_{NE} is used in formulating the device operation and performance. Experimentally, one usually measures ρ^a_{yy} and $\kappa_{xx}{}^*$. Therefore, the experimental figure-of-merit is z^{a*}_{NE}, i.e., $z_{NE} \le 1$. Theoretically, one usually calculates the thermal conductivity κ_{xx} and ρ_{yy}. Therefore, the theoretical figure-of-merit is also $z_{NE} \le 1$.
Here, in the following, we are assuming isothermal quantities for all material properties $\kappa_{xx}{}^*$, ρ_{yy}, and N_{yx}, i.e., they are the values measured for zero temperature gradient unless a temperature gradient in a direction is needed for the measurement. Further, we will be using the

$\kappa_{xx}{}^{*}$ and $z_{NE}{}^{*}$ in the equations. However, for convenience, we drop the superscript * from this point. As NE devices are usually assumed as a transverse isothermal cooler, there is no heat flow in the y and z directions; therefore, the device is generally made long in the y-direction with respect to x [20]. The net input power to the i^{th} stage, which is the difference between the input and output energy flow rate, can be expressed as [1]:

$$P^i = 2z\Delta x^i L_y E_y^i J_y^i \quad (4)$$

Similarly, for the next stage, $(i+1)^{th}$, the input power is [1]:

$$P^{i+1} = 2(z+\Delta z)\Delta x^{i+1} L_y E_y^{i+1} J_y^{i+1} \quad (5)$$

where Δx is the height, L_y is the length, z is the width of the corresponding stage, and Δz is the increment of the size in the z-direction with respect to the previous stage. For multistage devices, where all stages are physically connected, it is a reasonable consideration that the electric field across all stages must be the same. However, the current through each stage can be different because the stages are at different temperatures, and the electrical conductivity is a function of the temperature. To obtain optimum geometry, it is also essential to optimize the individual stages for the corresponding current density and voltage gradient [1]. Expressions of current density and voltage gradient for the optimized shaped device are given by [1]:

$$J_y = -\frac{\kappa_{xx}}{H_z N_{yx}} \frac{\Delta_x T}{T} \frac{(1+\delta)}{\Delta x} \quad (6)$$

$$E_y = -H_z N_{yx} \frac{\Delta_x T}{\Delta x} \frac{\delta}{(1-\delta)} \quad (7)$$

Here, it is imperative to mention that different expressions for optimum current densities were reported by Harman [1] and Hawkins et al. [20], which are essentially equal to each other. From the expressions of the electric field and the current density for the optimized shaped device, temperature-dependent Ohm's law for the NE device can be expressed as:

$$J_y = \frac{1}{\rho_{yy}\sqrt{1 - z_{NE}T}} E_y \quad (8)$$

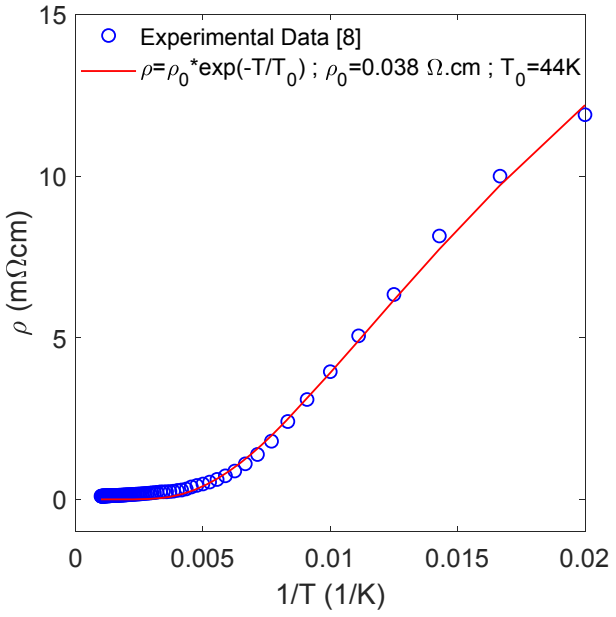

Figure 2: Resistivity (blue circle) of $Bi_{97}Sb_3$ as a function of reciprocal temperature with the corresponding exponential fit (red line).

Resistivity usually has a reciprocal relation with temperature [37]; however, the exponential relationship is more suitable for Bi_xSb_{1-x} semimetals in the cryogenic temperature range because the resistivity is mainly a function of carrier concentration, and the carrier excitation follows an exponential function vs. temperature. A good exponential fit to the experimental data is shown in Figure 2. Since a good thermomagnetic material must have a low extrinsic carrier concentration, the exponential relationship assumption is expected to be generally valid for other thermomagnetic coolers too. Therefore, the exponential function is used in the subsequent model calculations. According to this consideration, the resistivity in the temperature range of interest (Figure 2) may be written as, $\rho = \rho_0 e^{-T/T_0}$, where ρ_0 and T_0 are the material dependent constants. Replacing ρ in (8), we can write the expression for temperature-dependent Ohm's law for the i^{th} stage as:

$$J_y = \frac{e^{T_i/T_0}}{\rho_0\sqrt{1-zT}} E_y^i \qquad (9)$$

Assuming zT as a temperature-independent parameter and E_y constant for each stage, current density for $(i+1)^{th}$ stage can be written with respect to i^{th} stage as:

$$J_y^{i+1} = \frac{e^{T_{i+1}/T_0}}{\rho_0\sqrt{1-zT}} E_y^{i+1} = e^{T_{i+1}-T_i/T_0} J_y^i \qquad (10)$$

Simplifying (10), the ratio of the current densities of the $(i+1)^{th}$ and i^{th} stages can be expressed as:

$$\frac{J_y^{i+1}}{J_y^i} = e^{T_{i+1}-T_i/T_0} = 1 + \frac{\Delta T}{T_0} \qquad (11)$$

Here, $\Delta T = T_{i+1} - T_i$. To obtain the differential relation of eq. (1), we can write from (4), (5), and (10):

$$\frac{P^{i+1} - P^i}{P^i} = \frac{2(z+\Delta z)\Delta x^{i+1} L_y E_y^i J_y^{i+1} - 2z\Delta x^i L_y E_y^i J_y^i}{2z\Delta x^i L_y E_y^i J_y^i} \qquad (12)$$

Using (10), we can simplify the above expression by assuming a similar height (Δx) for all the stages:

$$\frac{P^{i+1} - P^i}{P^i} = \frac{\Delta P}{P} = \left(1 + \frac{\Delta z}{z}\right)\left(1 + \frac{\Delta T}{T_0}\right) - 1 \qquad (13)$$

Ignoring the second-order derivative terms after factor-multiplication, we can derive the following expression from (13):

$$\frac{\Delta P}{P} = \frac{\Delta z}{z} + \frac{\Delta T}{T_0} \qquad (14)$$

Finally, from (1) and (14), we can get the following differential relation:

$$\frac{dP}{P} = \frac{dz}{z} + \frac{dT}{T_0} = \frac{d\dot{\epsilon}}{\dot{\epsilon}} = \frac{dT}{TF(\delta)} = b \qquad (15)$$

Here, b is an arbitrary constant. To operate a multistage device at its optimum COP, one must adjust the intermediate stage temperatures according to the following relation [1]:

$$\frac{\Delta T^i}{\Delta x^i T^{i-1}} = \frac{\Delta T^{i+1}}{\Delta x^{i+1} T^i} = b', \qquad (16)$$

where, b' is another constant. Taking b' equal to $bF(\delta)$, we can write a generalized expression for (16) as [1]:

$$\frac{dT}{TF(\delta)} = bdx \qquad (17)$$

From (15) and (17), the following expression can be derived:

$$\frac{dz}{z} = bdx - \frac{dT}{T_0} \qquad (18)$$

Taking the integration on both sides of (18), finally, we get:

$$lnz = bx - \frac{T}{T_0} + c \qquad (19)$$

where c is a constant. Applying the boundary conditions, i.e., $T=T_c$ at $x=0$ and $T=T_h$ at $x=L_x$, we can find b and c. By inserting them in (19), we can write:

$$ln\frac{z(x)}{z(0)} = \frac{x}{L_x} ln\frac{z(L_x)}{z(0)} + \frac{x}{L_x}\frac{T_h - T_C}{T_0} - \frac{T - T_C}{T_0} \qquad (20)$$

Eq. (20) is the corrected function for the infinite stage geometry. Compared with Harman's shaping function [1],

$$ln\frac{z(x)}{z(0)} = \frac{x}{L_x} ln\frac{z(L_x)}{z(0)} \qquad (21)$$

We can introduce the corrected shaping function as:

$$ln\frac{z(x)}{z(0)} = \frac{x}{L_x} ln\frac{z(L_x)}{z(0)} + C \qquad (22)$$

in which the correction term, C, is:

$$C = \frac{x}{L_x}\frac{T_h - T_C}{T_0} - \frac{T - T_C}{T_0} \qquad (23)$$

According to the above expression, C has a contribution from temperature-dependent and material property-dependent corrections. From (23), it can be seen that hot side temperature, cold side temperature, the device length, the spatial temperature profile of the device, and the T_0 parameter can deviate the optimum shape of the multistage device from that of Harman's shaping function. Corrected infinite stage function can be reduced to Harman's infinite stage function with dT = 0.

Numerical Framework

In this section, we develop a generalized numerical model based on the device fundamental equations [40]. All material properties are taken temperature-dependent. The model is solved to analyze and compare the different geometries of the NECs. The numerical framework is based on the thermodynamic relations of a single-stage parallelepiped NE device [40], which is then extended to include the current density and spatial temperature distribution along the x-direction of a cooler in a self-consistent manner. In transverse isothermal thermomagnetic coolers, $\nabla_y T = 0$ and J_x = 0 conditions are usually applied to the thermodynamic relations [40]. The interdependent temperature gradient and the heat flow density of individual stages are self-consistently solved across the target geometry. An equivalent electrical circuit model (shown in Figure 1) is used to simplify the calculations. In this model, heat-flow and temperature are represented by electrical current and voltage sources, respectively. The thermal resistance of each stage is modeled by electrical resistance. The temperature profile across the cooler is calculated iteratively, considering the interdependent heat current density and temperature.

The temperature at j^{th} stage can be expressed as:

$$T_j = T_{j+1} - {R_{th}}^j \left(\sum_{i=1}^{j} {Q_{Ec}}^i - \sum_{i=1}^{j-1} {Q_{Eh}}^i - Q_{in} - \sum_{i=1}^{j} {Q_J}^i + \frac{{Q_J}^j}{2} \right) \quad (24)$$

where R_{th} is the thermal resistance of a single stage at the isothermal condition. Q_{Ec} and Q_{Eh} are the Ettingshausen heat flow density at the cold side and hot side of a single-stage, respectively. Q_{in} is the input heat flow density, and Q_J is the Joule heat flow density. Here, R_{th} is calculated from $R_{th} = 1/(\kappa_{xx}(1 - z_{NE}^* T)) \times \Delta x_i/(L_y L_{z_i})$ [20], in which T is the average temperature of the stage. We have considered the second definition of the figure-of-merit, ${z_{NE}}^*$, as described earlier in the manuscript, in the calculation of the thermal resistance R_{th} and any other device properties. From (24), the expression for cold side temperature can be written as:

$$T_c = T_h - \sum_{j=1}^{N} {R_{th}}^j \left(\sum_{i=1}^{j} {Q_{Ec}}^i - \sum_{i=1}^{j-1} {Q_{Eh}}^i \right) + \sum_{j=1}^{N} {R_{th}}^j Q_{in} + \sum_{j=1}^{N} {R_{th}}^j \sum_{i=1}^{j} {Q_J}^i - \frac{1}{2} \sum_{j=1}^{N} {R_{th}}^j {Q_J}^j . \quad (25)$$

Finally, the input heat current density can be expressed as:

$$Q_{in} = \frac{1}{\sum_{j=1}^{N} {R_{th}}^{j}} \left(T_c - T_h + \sum_{j=1}^{N} {R_{th}}^{j} \left(\sum_{i=1}^{j} {Q_{Ec}}^{i} - \sum_{i=1}^{j-1} {Q_{Eh}}^{i} \right) - \sum_{j=1}^{N} {R_{th}}^{j} \sum_{i=1}^{j} {Q_J}^{i} + \frac{1}{2} \sum_{j=1}^{N} {R_{th}}^{j} {Q_J}^{j} \right) \quad (26)$$

In the following, we will study and compare the performance of different shaped devices. Figure 3 illustrates the geometry of studied devices. To compare the different device geometries, we chose the device parameters as L_x = 0.5 cm, L_y = 1 cm, L_z at cold side = 0.1 cm, T_h = 150K, and z_{ratio} = 5. All devices are divided into 500 single parallelepiped stages. The physical properties of single-crystal $Bi_{97}Sb_3$ were assumed in the numerical model [20]. The cooling temperature, the heat flow density, and COP were compared for the different geometries. Furthermore, the COP and dT/T across the device (versus x) was calculated to validate the assumptions made in deriving the optimum geometry. The detailed discussion is presented in the following section.

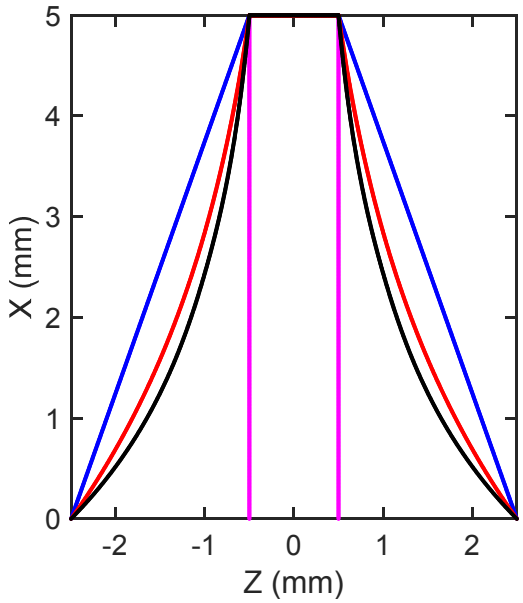

Figure 3: Different geometries used to compare NE device performance, which includes rectangle (pink), trapezoid (blue), Harman's infinite stage (red), and temperature-dependent corrected infinite stage (black). The corrected infinite stage aligns with Harman's at dT = 0. With the increase of dT, the corrected shaped device becomes thinner in the middle. According to (25), device length can also affect the optimum shape deviation.

Result and Discussion

The device characteristics were calculated numerically using temperature-dependent material properties of single crystal $Bi_{97}Sb_3$. Quite often, in the literature, only the temperature difference is reported as a function of current for different hot side temperatures [20,38], and the COP or heat flow densities are usually neglected due to their complicated calculations [20]. Therefore, we demonstrated the usefulness of the model by calculating all the three quantities for different geometries and under different conditions. Four different shapes were modeled, namely, a rectangular cuboid, a trapezoidal prism, Harman's infinite stage, and the corrected temperature-dependent infinite stage device.

Figure 4 illustrates the temperature map of differently shaped NE devices superimposed on their geometrical shapes for the maximum temperature difference (ΔT_{max}). In all devices, the hot side is at the bottom of the devices, which was kept fixed at 150 K. Therefore, heat flow occurs in a downward direction from the cold to the hot side. The temperature profile for different geometries can be compared to the figure. In the rectangular cuboid, the temperature increases more quickly compared to other geometries below the top surface. Therefore, the cooling performance of shaped devices is better than that of a rectangular-shaped device.

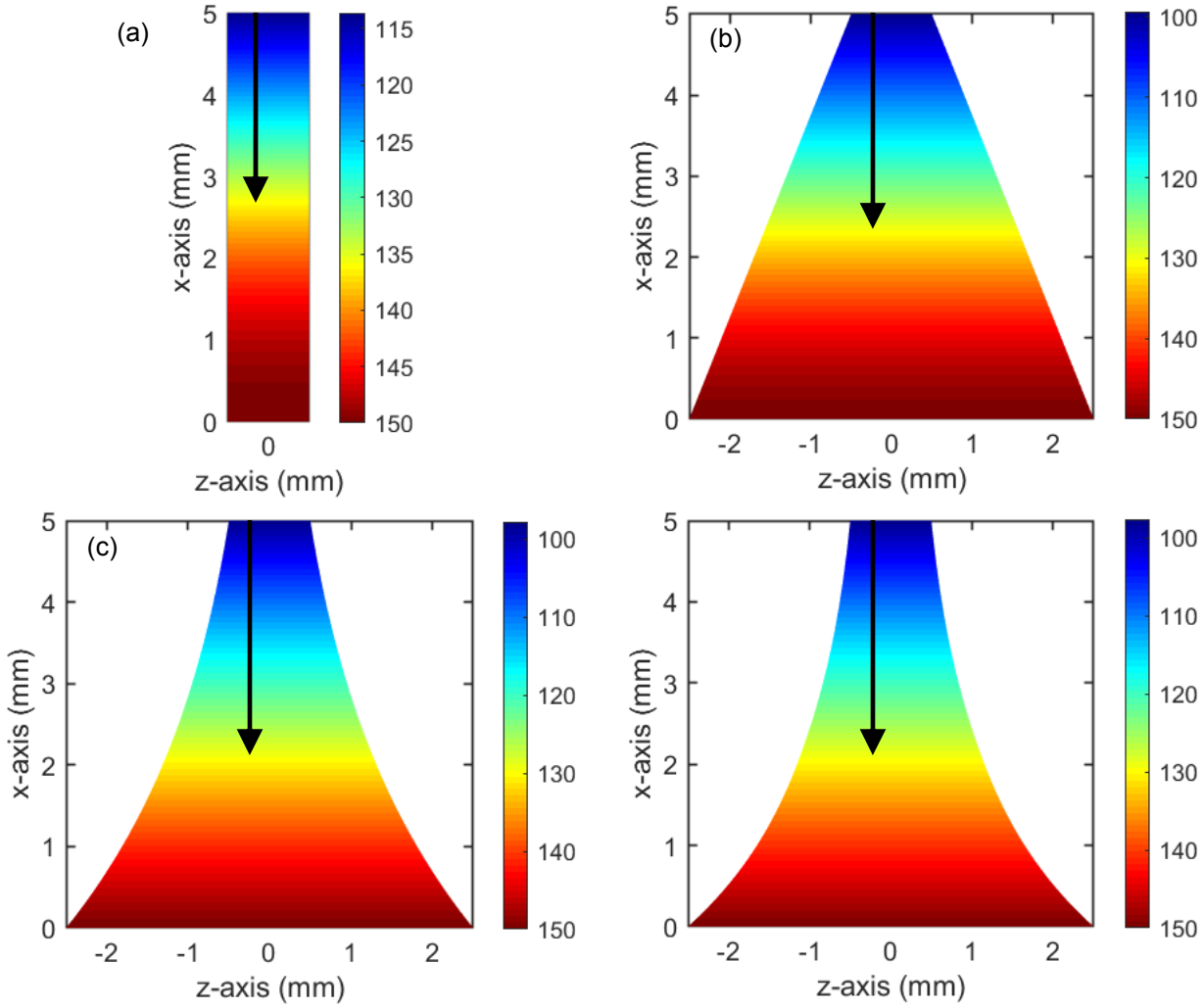

Figure 4: Spatial Temperature map with cooling depth (arrow) at maximum temperature difference in differently shaped NE devices: (a) thin rectangular cuboid, (b) trapezoidal prism, (c) Harman's infinite stage device, and (d) the corrected infinite stage. The cold and hot side widths are assumed to be 1 mm and 5 mm, respectively, and the hot side temperature is fixed at 150 K.

A similar kind of comparison is demonstrated in Figure 5, where temperature variation along the x-axis for all devices is plotted at two temperature differences of ΔT = 0K and ΔT_{max}. Temperature variation is shown for both maximum heat flow, Q_{max}, and optimum COP conditions. It can be seen from both figures that the temperature at any x point inside the device is higher in the rectangular device compared to the others. Therefore, it is expected that the cooling performance in the shaped devices should be better than the rectangular device.

Moreover, the spatial temperature profile becomes linear in infinite staged devices at ΔT_{max}. Generally, ΔT = 0K happens when the device works at its maximum cooling power, Q_{max}. All Ettingshausen devices, except the corrected infinite staged device, show higher temperatures inside the device than the ends under Q_{max} condition at ΔT = 0K. For COP_{opt} condition, the inner temperature of all staged devices, except rectangle one, drops compared with the end temperatures at ΔT = 0K. Temperature variation trend along x-axis under ΔT_{max} condition for all devices is in agreement with the observed trends in Figure 4.

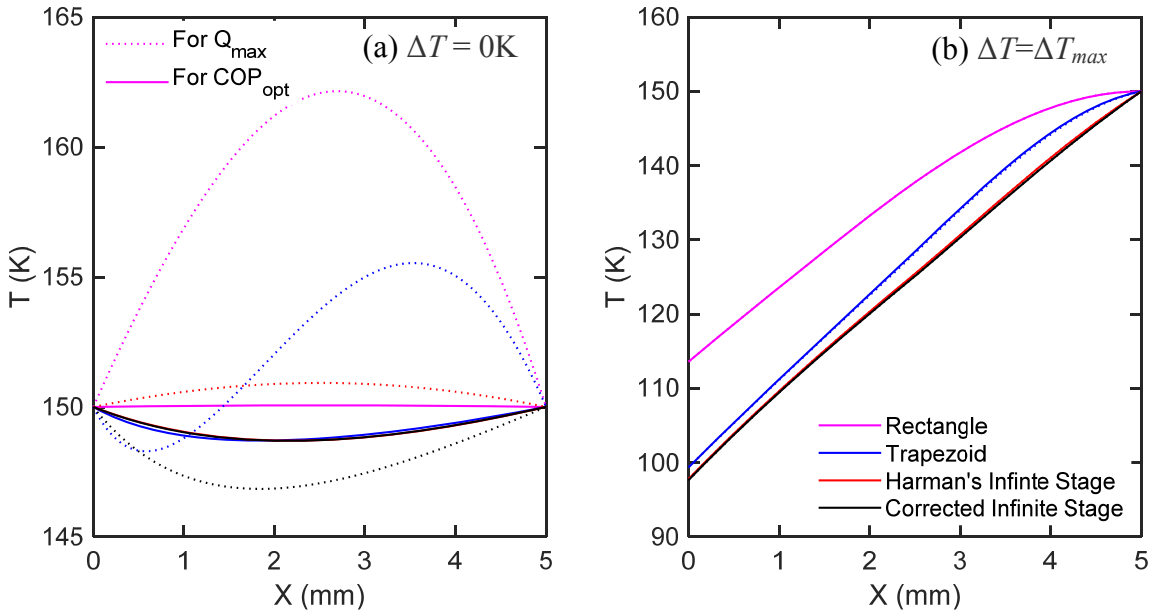

Figure 5: The temperature variation along x-axis for different devices at (a) ΔT = 0K and (b) ΔT_{max}.

The typical performance indicator for Ettingshausen devices is the temperature difference as a function of operating current. To evaluate the devices' performances with different geometric shapes, we plotted the temperature difference, ΔT, as a function of current in Figure 6. As expected, shaped NE devices provide larger ΔT than rectangular shaped devices, which was also confirmed in previous figures. For rectangular devices, ΔT_{max}~36K is obtained at 7A, while ΔT_{max}~50K for trapezoidal at 32A, ΔT_{max}~52K for Harman's infinite stage at 25A, and ΔT_{max}~52.3K for corrected infinite staged NE device at 24A are obtained. The results also show good agreement with the previously published data [20,38]. After ΔT_{max}, ΔT decreases with the increase of the electrical current due to the dominancy of the Joule heating over Ettingshausen cooling. The corrected infinite stage gives a slightly higher ΔT_{max} at the lower current than Harman's infinite stage device. As we will discuss, the corrected infinite stage device can operate at a simultaneously higher COP and heat flow density compared to other geometries. Therefore, to evaluate the device performance, COP and heat flow density are also important parameters along with the highest achievable ΔT. Moreover, at maximum ΔT, heat flow density, hence COP, is zero. As mentioned earlier, no prior reports were found for the heat flow and COP of different geometries so that this study can provide a benchmark for future works. Such calculations are comparatively more extensive than ΔT and require detailed analysis. In the following, we will demonstrate both COP and heat flow density for different shaped devices and compare their

performances. Both heat flow and COP are shown for two temperature differences lower than ΔT_{max}, namely, ΔT=10K and ΔT=50K for a low and a high-temperature difference condition.

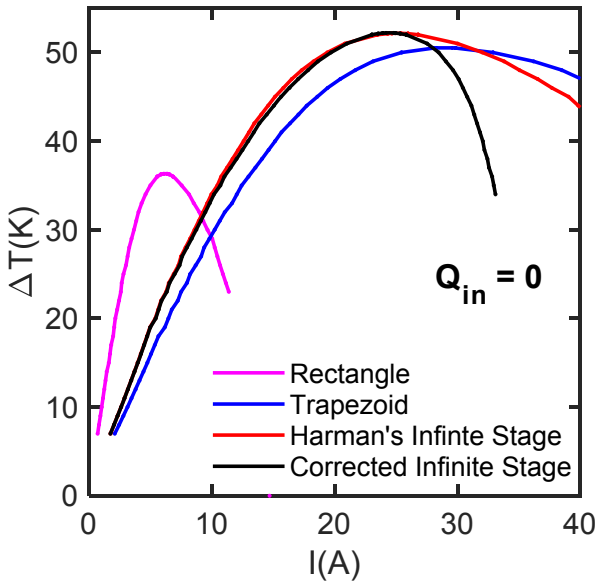

Figure 6: Illustration of temperature difference (ΔT) versus current (I) for different shaped NE devices: rectangular, trapezoidal, Harman's infinite, and corrected infinite staged device derived in this work.

Heat flow density from the cold side to the hot side as a function of the electrical current is calculated at ΔT = 10K and ΔT = 50K for all NE devices. Heat flow inside a NE device consists of both Joule and Ettingshausen components, as shown in Figure 1. The heat flow density for each NE device is higher for smaller ΔT as expected, and shown in Figure 7(a). With the increase of ΔT to 50K, the heat flow reduces significantly, as shown in Figure 7(c). At ΔT = 50K, heat flow density becomes negative for rectangular NE devices, as ΔT_{max}≈36K for this device. Therefore, heat flow density for the rectangular NE device is not shown in Figure 7(c) and (d). As mentioned earlier, heat flow density shows a decrease after a maximum value with the increase of the current density, which is related to the domination of the Joule heating over the Ettingshausen cooling. While shaped NE devices show better heat flow capacity than the rectangular one, the trapezoidal NE device has a higher heat flow density than that of the infinite staged devices at ΔT = 10K, which corresponds to its larger electrical current (larger input power) as shown in Figure 6. Note that Ettingshausen's heat flow density is proportional to the current, while Joule heat flow density is proportional to the current square. Therefore, the heat flow density trend follows the trend of Ettingshausen heat flow density at the lower current range, and at higher currents, the total heat flow density follows the pattern of the Joule heating. The corrected infinite staged device gives higher heat flow density at around 50K than that of the trapezoid and Harman's infinite-stage device, and the peak happens at a lower electrical current, which can be attributed to the more accurate consideration of the Joule heating in designing this device. At ΔT = 10K, the corrected infinite staged NE device also has higher heat flow density than that of Harman's infinite stage devices at a lower current. As we will discuss, this results in a higher COP for the corrected infinite stage device. Here, it is essential to mention that the corrected staged device is thinner than both trapezoid and Harman's infinite stage devices; hence,

it pumps more heat with less amount of material. It should be noted that, according to eq. (20), the optimum geometry is a function of both T_C and ΔT. Therefore, the corrected infinite staged NE device optimized for ΔT=50K may not be optimum for a different ΔT (or T_C).

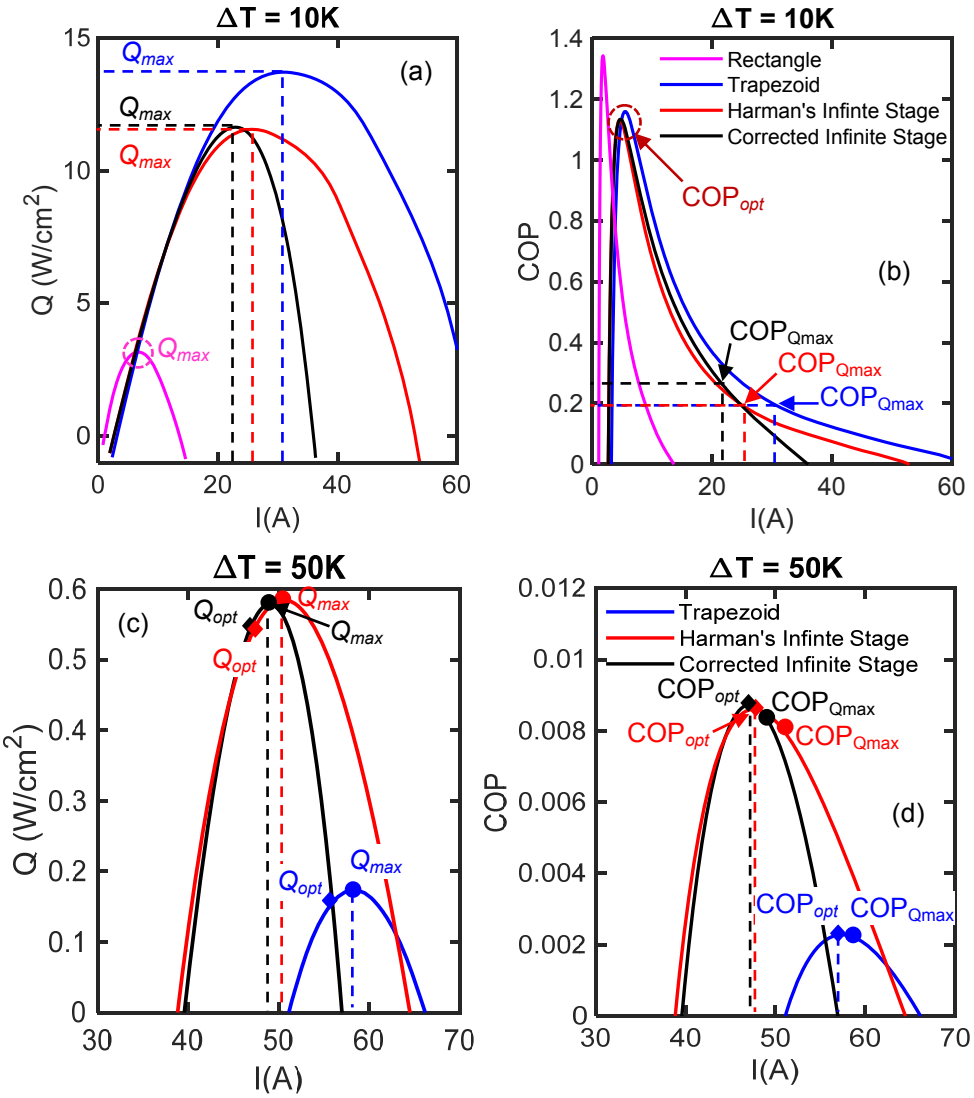

Figure 7: Heat flow density ((a) and (c)) and COP ((b) and (d)) as a function of driving current for different geometric-shaped NE devices at ΔT = 10K ((a) and (b)), and ΔT = 50K ((b) and (d)).

For evaluating the performance of the shaped devices, a comparison of the COPs is also critical, shown in Figure 7(b) and (d). COP versus current for each shaped device at a given ΔT is calculated. Here, the heat flow with respect to the electrical current is adjusted so that the ΔT remains fixed. At a lower temperature difference (ΔT =10K), the rectangular NE device shows a higher COP_{opt} of around 1.35 at 1.8A with a significantly lower heat flow density (around 1W/cm^2), which is not desirable for practical applications. However, rectangular devices can provide a higher heat flow density of around 3.2W/cm^2 at around 6.7A and COP of 0.35. On the other hand, corrected shaped NE devices give higher COP_{Qmax} (around 0.3) at a lower current (around 20A) than other shaped NE devices (around 0.2 for both Trapezoid and Harman's infinite-stage shaped devices). Compared to the trapezoid NE device, the corrected shaped

device provides around 30% higher COP with around 18% less heat flow density at ΔT =10K. Despite showing higher COP at the low-temperature difference, the COP of rectangular devices drops sharply with the current. At lower ΔT and COP_{opt} condition, Q_{opt} is much lower than Q_{max}, and all shaped devices provide similar Q_{opt} performance. In general, shaped NE devices have a higher COP than those of rectangular NE devices at a particular current value and higher temperature difference, consistent with the previous results and theory [20,38]. At 10K, the trapezoidal device has slightly higher COP at a slightly higher current with similar heat flow density, as seen in Figure 7(a) and (b). But, at a larger ΔT, infinite stage devices show much better COP than the trapezoidal device. At 50K, both infinite stage devices pump more heat flow at a lower current than the trapezoidal device (Figure 7), which results in higher COPs. Moreover, corrected infinite staged devices can pump slightly higher heat at a slightly lower current than Harman's infinite stage device, which gives it a somewhat higher COP. While the COP_{Qmax} for the Harman's infinite stage device is about 0.2 at ΔT = 10K, the corresponding value is about 0.28 for the corrected infinite stage device, i.e., 40% improvement. At a 50K temperature difference, the corrected shaped device provides around 5% higher COP_{Qmax} than Harman's infinite shaped device. Both infinite staged devices show similar COP_{opt} with similar Q_{opt} performance. As mentioned, COP can be two types, namely, COP_{Qmax} and COP_{opt}. To determine the optimum operating condition for a NE device, we must consider both the current and the heat flow density. Heat flow density should be maximized as a function of the current or the desired temperature differential. Then, the corresponding COP is calculated versus the current density and heat flow conditions.

One can see from Figure 7 that the efficient operation of a NE cooler typically requires a high current at a low voltage. Depending on the cooler's size, the current and voltage scale with the cross-section and length of the cooler, respectively. The voltage scales with *z*, which does not affect the cross-section, hence, the optimum current. Indeed, this is one of the advantages of NE coolers compared to TECs, as the same current can cool larger areas by simply scaling the device in the z-direction. The current scales with the cross-section in the xy-plane and can be much smaller for a miniature cooler, e.g., for on-chip cooling of FPAs or electronic devices. The optimum current density is in the order of a few 100 A/cm^2, which is practical for many devices.

Finally, the contact resistance usually is less an issue for NECs compared to TECs because (a) NECs have only two contacts, while TECs have many, and (b) NECs can be made long (in the *z*-direction); as such, their resistance dominates over the contact resistance. For instance, the resistance of the thin rectangular NEC (5×10×2 mm^3) is around 0.04 Ω at 100K. The typical metal-semiconductor contact resistance for the given cross-section is ~0.00001 Ω, assuming $\rho=10^{-6}$ Ωcm^2, which is comparatively negligible. According to Figure 7, rectangular devices can operate at lower current, i.e., 6.7 A for Q_{max} or 1.8 A for the COP_{opt} at ΔT=10 K. But unlike shaped NECs, the ΔT of the rectangular device is limited by $^1/_2\, z_{NE} T_c^2$ or $^1/_2\, z_{NE}^* T_h^2$ [37,41] independent from the dimensions.

To show the concept of optimum device operating conditions, we illustrate some critical parameters in Figure 8. Figure 8(a) shows the heat flow density, Q, which is maximized as a function of current density for each ΔT, Figure 8(b) provides COP versus ΔT for maximum Q,

i.e., COP_{Qmax}, and the corresponding current density, and Figure 8(c) gives current density that maximizes Q. On the other hand, Figure 8(d) shows the heat flow density, Q, versus ΔT which maximizes the COP, i.e., Q_{opt}, as a function of current density, Figure 8(e) provides COP_{opt} versus ΔT for optimum Q and the corresponding current density, and Figure 8(f) illustrates current density that optimizes Q. As expected, maximum heat flow density and COP both decrease linearly with the increase of ΔT and approach zero at ΔT_{max}. In Figure 8(b), the rectangular device shows higher COP_{max} at lower ΔT, which is also seen in Figure 7. Note that COP is presented as a function of current in Figure 7, while COP_{Qmax} at ΔT=10K is for the maximum heat flow density at the same temperature difference (shown in Figure 7). According to Figure 7, the heat flow density of different NE devices at ΔT=10K maximizes at different current, which corresponds to different COPs in Figure 8. In general, higher COP_{Qmax} at lower temperature difference for rectangles can be related to its lower current density at the cost of lower heat flow capacity, which is not always desired for practical use. In contrast, shaped NE devices can take higher heat at the expense of higher current density, which makes them better for higher ΔT applications. Importantly, the corrected infinite stage device always shows better COP than that of other shaped devices, as it carries more heat at a less current.

Interestingly, the COP of the trapezoid is slightly higher at low ΔTs and only marginally lower at high ΔTs than that of the infinite staged devices. Therefore, the trapezoidal device can be a better option for practical applications due to its simpler structure. At high ΔTs, the COP of both infinite stage devices becomes higher due to the higher heat flow at a lower driving current. Rectangular device performance shown in Figure 8 agrees with previous results [20]. We have not seen any report of the COPs of other devices in the literature.

Optimum heat flow and COP show different trends than Q_{max} and COP_{Qmax}. Optimum heat flow first increases with an increase in ΔT, but above ΔT>30K, it shows a rapid decrease with a further rise in ΔT. On the other hand, COP_{opt} of all Ettingshausen devices at ΔT<20K show approximately similar values. At a lower temperature difference, COP_{opt} is higher than unity for all devices, and it increases rapidly as ΔT approaches zero, as also shown in Figure 10. Above ΔT=25K, while the shaped devices exhibit approximately the same COP_{opt}, they are significantly higher than the COP_{opt} of the rectangular device. This trend is expected as the shaped devices always carry higher heat flow density than the rectangle device. The trapezoidal device shows somewhat better performance in terms of Q_{opt} up to approximately ΔT=40K at the cost of a higher current. At ΔT>40, however, the COP_{opt} of the trapezoidal device drops rapidly below those of the infinite stage devices. The corrected infinite stage device carries higher optimum heat flow at a slightly higher current than Harman's infinite stage device while providing almost similar COP_{opt}.

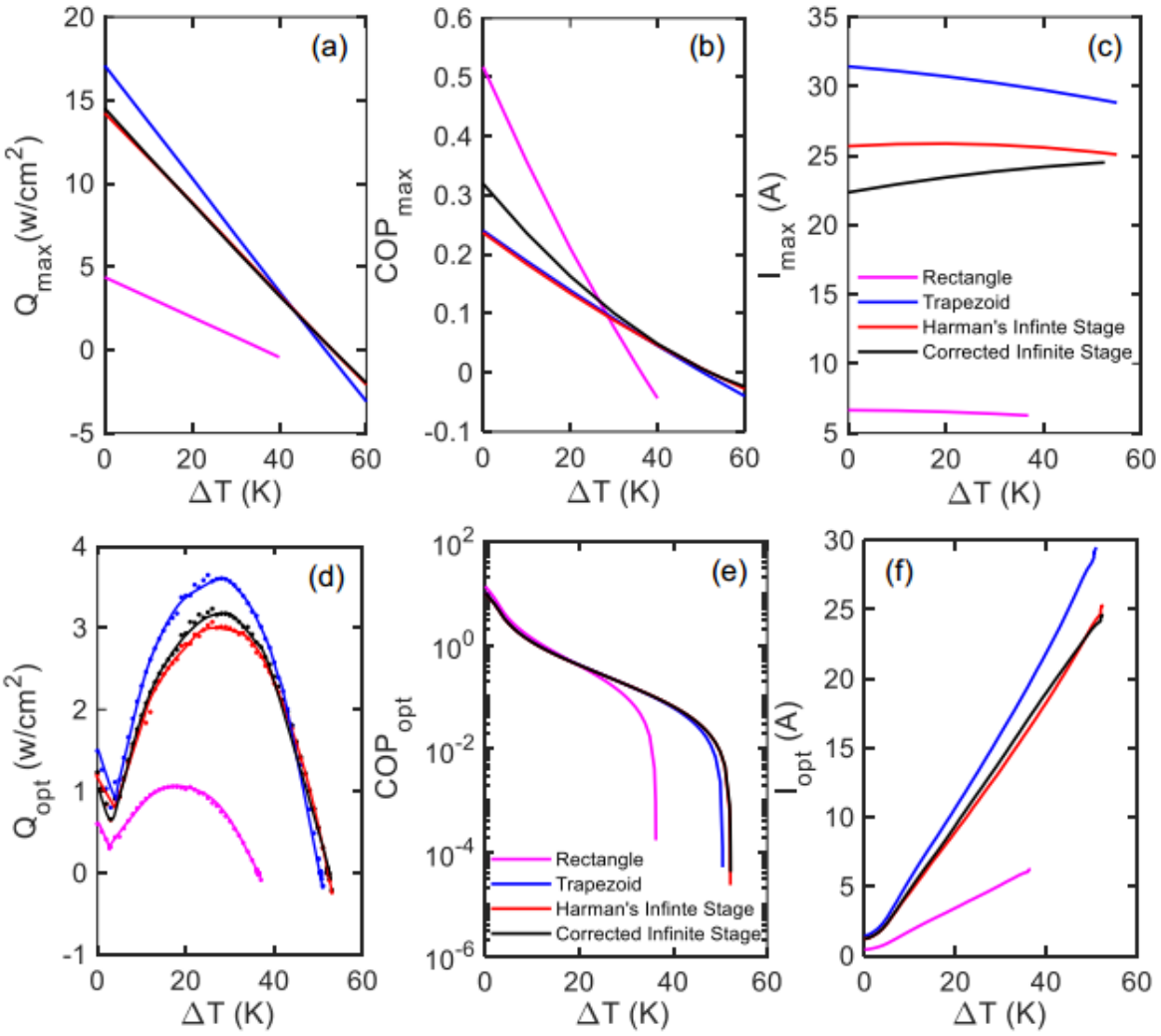

Figure 8: (a) Maximum heat flow density versus temperature differential when the current is adjusted to achieve maximum Q, (b) COP at maximum heat flow density, (c) Current density at maximum heat flow density, (d) optimum heat flow density versus temperature differential when the current is adjusted to achieve maximum COP, (e) COP_{opt} versus temperature differential, and (f) the corresponding current.

higher current density at a particular COP. A similar characteristic is also observed in Figure 8(a) that trapezoidal devices can give higher heat flow at a specific temperature differential. Like Figure 7, COP_{Qmax} and COP_{opt}, as shown in Figure 9(a), are significantly different at small Δ*T*s. This is usually not the case for TE or Peltier coolers. On the other hand, at larger ΔT, infinite staged devices have significantly higher COP with higher heat flow density than that of trapezoid devices. Between the Harman's and corrected infinite stage devices, the corrected infinite stage devices have slightly higher COP for the same heat flow density condition. Therefore, the corrected infinite staged device shows overall better performance than the other shaped devices of similar material at higher ΔT. At higher ΔT, both COP_{Qmax} and COP_{opt} have similar values, which can also be seen in Figure 11.

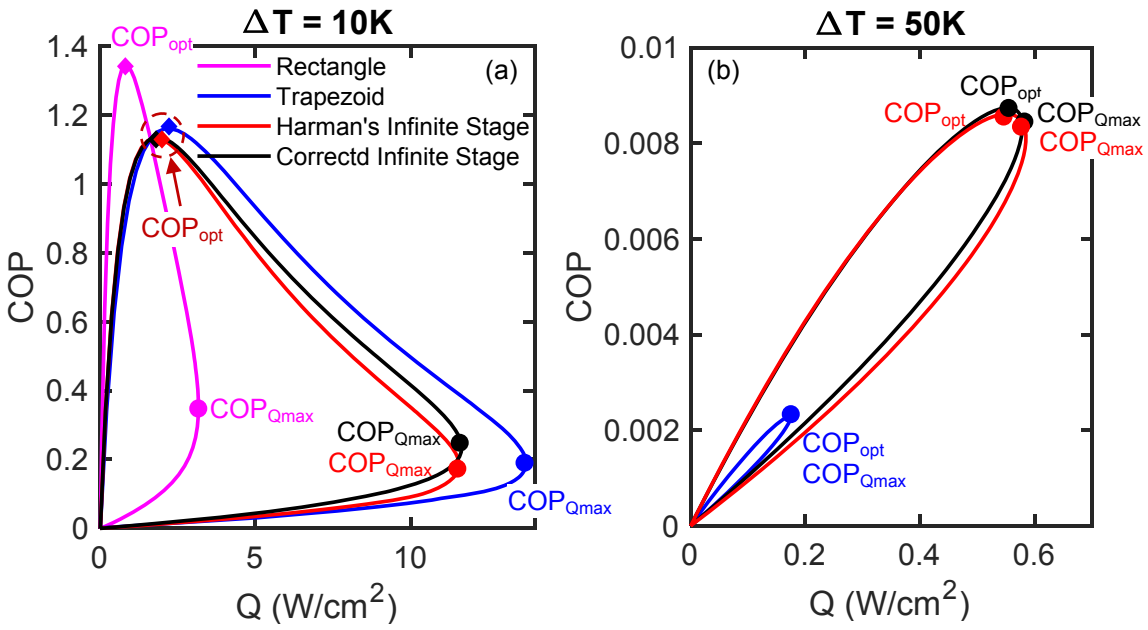

Figure 9: COP versus heat flow density for different geometric-shaped Nernst-Ettingshausen devices at ΔT = 10K (a) and ΔT = 50K (b).

Figure 10 and Figure 11 illustrate the overall comparison of the device performance among different shaped devices. Figure 10 demonstrates COP and heat flow density with respect to the electric field and temperature difference. COP as a function of electric field and ΔT looks similar for all NE devices with a divergent point at lower electric fields and lower Δ*T*s. COP drops sharply with the increase in both temperature difference and the electric field. On the other hand, heat flow density as a function of the temperature difference, and the electric field demonstrates similar trends observed in earlier figures. Rectangle NE devices provide less heat flow density, while trapezoid NE devices show better heat pump capability than others at lower temperatures at the cost of a higher current. Corrected infinite stage device is better in terms of the heat pump at higher operating temperature differential. Figure 11 compares the temperature differential as a function of COP and heat flow density under maximum COP and maximum Q conditions for all the devices. Rectangular devices show almost similar characteristics of ΔT for both conditions, while shaped devices have different trends of ΔT under different circumstances. Similar ΔT_{max} is obtained at maximum Q and COP conditions for each device. Like the earlier discussion, infinite stage devices show better performances at larger ΔT, while corrected infinite stage devices can carry more heat flow at higher COP than the other devices. This improvement supports the argument that Harman's infinite shaped expression was formulated based on some simplifying assumptions, which overestimated the Joule heating of the device. Among all the geometries, the trapezoidal device gives consistent optimum performance in terms of the heat flow and COP over the whole range of ΔT at the cost of slightly smaller ΔT_{max}. The trapezoidal device, considering the complexity of making infinite staged devices, can be a better option for practical cooling applications.

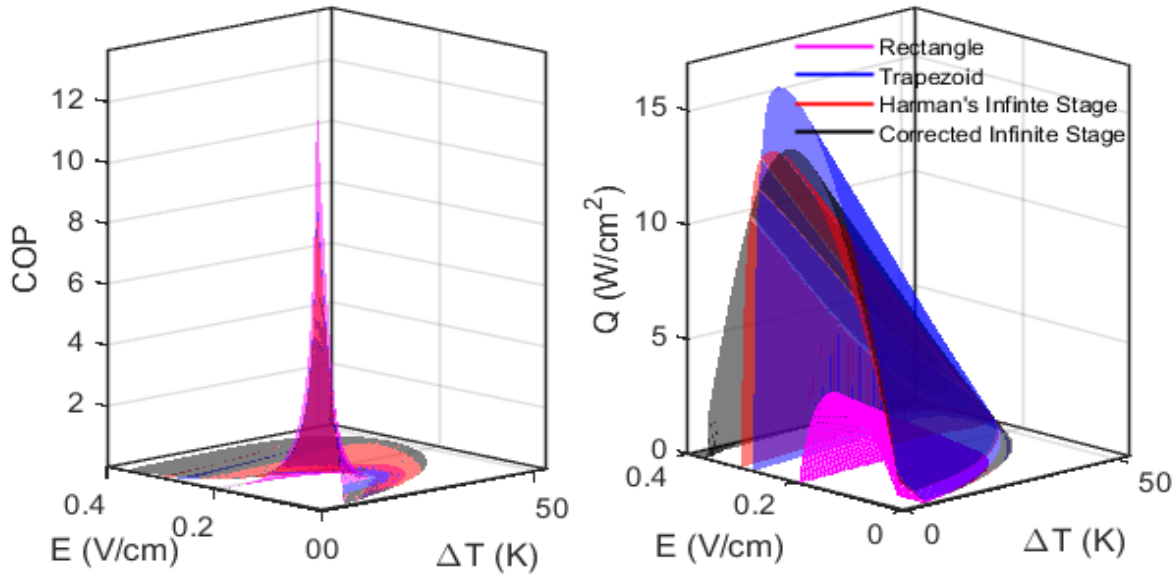

Figure 10: (a) COP and (b) heat flow density as a function of applied electric field and temperature differential for different shaped devices.

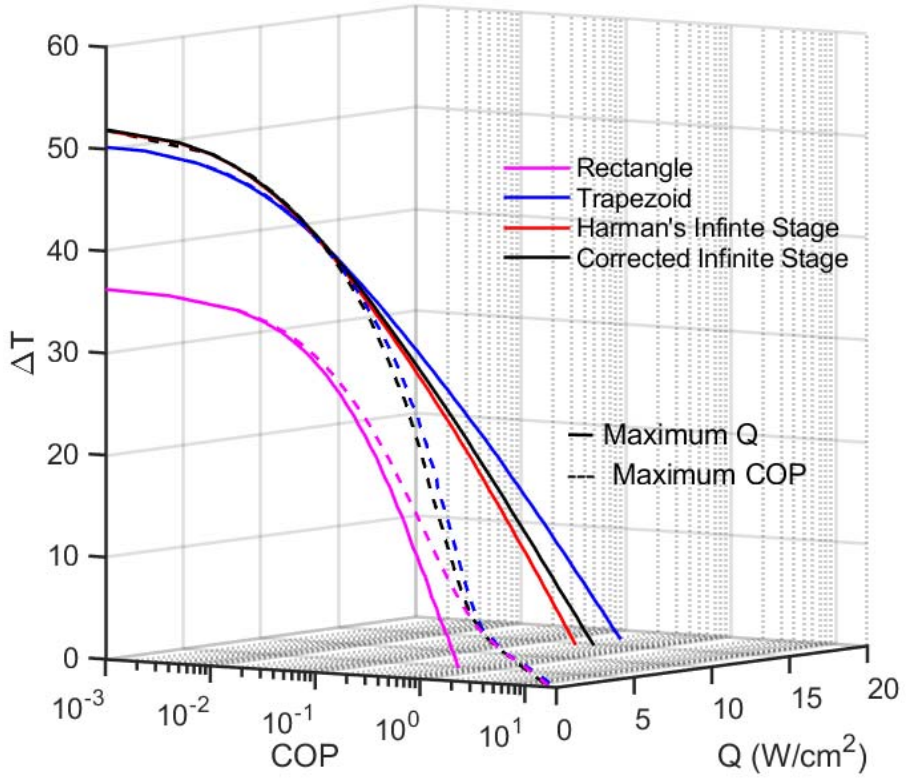

Figure 11: Temperature differential as a function of COP and heat flow density for different NE devices under maximum COP and maximum heat flow conditions.

Conclusion

The prospect of superconductors and spin-based applications at cryogenic temperature range guided the scientific community to observe several exotic thermomagnetic effects coming from spin and quantum effects [42-44] which provide superior performance in solid-state cryocoolers [45,46]. We derived a modified expression for the shaping function of the infinite stage Nernst-Ettingshausen coolers, which considers the temperature-dependent material resistivity, the device size, and the temperature conditions for designing a fully optimized cooler. In this derivation, some ideal assumptions made by Harman was corrected to obtain the modified infinite stage shape function. The corrected shape agrees with Harman's shape at zero temperature difference and temperature-independent resistivity conditions and differs otherwise. A numerical model was further introduced that can consider all temperature-dependent material properties and for any given shape device. A case study based on BiSb material was discussed to analyze and compare the performance of different shaped coolers. The corrected infinite stage device was found better in terms of the maximum heat flow density and coefficient of performance (COP) at higher temperature differentials. A complete comparison of the device performance among different shaped devices was provided to guide the selection of an optimum device structure based on the cost and applications. The trapezoidal device, while having a more straightforward shape for fabrication purposes, can provide consistent cooling performance at the expense of a slightly lower temperature differential.

Acknowledgments

This work is partially supported by the National Science Foundation (NSF) under grant numbers ECCS-1351533, ECCS-1515005, and ECCS-1711253 and the Air Force Office of Scientific Research (AFOSR) under contract number FA9550-19-1-0363.

Appendix

Harman's Derivations for the Infinite Stage NE Cooler

Based on the energy conservation principle, the rate of the output energy flow ($\dot{\epsilon}$) from the (i+1)th stage should be equal to the sum of the rate of the input energy flow coming from the previous i^{th} stage and total power input (P) to the (i+1)th stage. The conservation law also ensures that the output energy of the i^{th} stage is equal to the input energy of the (i+1)th stage. Considering these relations, we can write the energy balance for the (i+1)th stage as:

$$\dot{\epsilon}_{out}^{i+1} = P^{i+1} + \dot{\epsilon}_{in}^{i+1} = P^{i+1} + \dot{\epsilon}_{out}^{i} \quad (a1)$$

Considering, $\dot{\epsilon}_{out}^{i} = \dot{\epsilon}^{i}$ and $\dot{\epsilon}_{out}^{i+1} = \dot{\epsilon}^{i+1}$, eq. ($a$1) can be written as:

$$\dot{\epsilon}^{i+1} = P^{i+1} + \dot{\epsilon}^{i} \quad (a2)$$

Now, according to the definition of the COP of the (i+1)th stage (COP is the ratio of the energy flow rate at the cold side and input power), we can write:

$$COP^{i+1} = \frac{\dot{\epsilon}^{i}}{P^{i+1}} = \frac{\dot{\epsilon}^{i}}{\dot{\epsilon}^{i+1} - \dot{\epsilon}^{i}} \quad (a3)$$

Similarly, COP for the i^{th} stage can be written as:

$$COP^i = \frac{\dot{\epsilon}^{i-1}}{P^i} = \frac{\dot{\epsilon}^{i-1}}{\dot{\epsilon}^i - \dot{\epsilon}^{i-1}} \qquad (a4)$$

Here, $\Delta P^{i+1} = P^{i+1} - P^i$. Therefore, eq. (*a*3) can be rewritten as:

$$COP^{i+1} = \frac{\dot{\epsilon}^{i-1} + P^i}{P^i + \Delta P^{i+1}} \qquad (a5)$$

For deriving the optimum device shape, another essential assumption is the requirement of an equal individual COP among all the stages. Hence, $COP^{i+1} = COP^i$ which requires

$$COP^i = \frac{P^i}{\Delta P^{i+1}} = \frac{P^i}{P^{i+1} - P^i} \qquad (a6)$$

From eqs. (*a*4) and (*a*6), a differential relation can be obtained as:

$$\frac{dP}{P} = \frac{d\dot{\epsilon}}{\dot{\epsilon}} \qquad (a7)$$

Moreover, for a parallelepiped-shaped NE stage (see Figure 1), the input heat flux density (Q_{in}) and input power (P) can be found from the thermodynamic relations [40], and can be written as [20]:

$$Q_{in} = \frac{E_y}{\rho_{yy}} B_z N_{yx} T_0 - \frac{1}{2}\frac{E_y^2 a}{\rho_{yy}} - \left(1 - z_{yx}\bar{T}\right)\kappa_{xx}\frac{\Delta T}{a} \qquad (a8)$$

$$P = \frac{E_y^2 ac}{\rho_{yy}} + \frac{B_z N_{yx}}{\rho_{yy}} \Delta T c \qquad (a9)$$

Here, E is the electric field, B is the magnetic field, ρ is the resistivity, κ is the thermal conductivity, N is the Nernst coefficient, T_0 is the temperature on the cold side, T_L is the temperature on the hot side, $\Delta T = T_L - T_0$ and $\bar{T} = (T_L + T_0)/2$, z is the figure-of-merit, and a, b, and c are the device length along the x, y, and z-axis. Now, according to the definition, COP can be written as:

$$COP = \frac{Q_{in} bc}{P} \qquad (a10)$$

The COP in eq. (*a*10) can be maximized for the optimum electric field, which provides a simplified expression for optimum COP:

$$COP_{max} = \frac{T_0}{\Delta T}\frac{(1 - \delta\frac{T_L}{T_0})}{(1 + \delta)} = \frac{T_0}{\Delta T} F(\delta) \qquad (a11)$$

To derive the optimum geometry, we must optimize the individual COPs [1]. From eqs. (*a*4), (*a*6), and (*a*11), the final differential relation can be written as:

$$\frac{dP}{P} = \frac{d\dot{\epsilon}}{\dot{\epsilon}} = \frac{dT}{TF(\delta)} \qquad (a12)$$

Following the similar steps given in the Derivation section, a slightly different differential relation was obtained by Harman, which is [1]:

$$\frac{dP}{P} = \frac{dz}{z} = \frac{d\dot{\epsilon}}{\dot{\epsilon}} = \frac{dT}{TF(\delta)} = b \qquad (a13)$$

Again, based on similar conditions given in the Derivation section, the Harman's infinite shape function can be found from eq. (a13), which is [1]:

$$ln\frac{z(x)}{z(0)} = \frac{x}{L_x} ln\frac{z(L_x)}{z(0)} \qquad (a14)$$

References

1. T. C. Harman, "Theory of the infinite stage Nernst-Ettingshausen refrigerator," *Adv. Energy Convers.,* 3(4), 667-676 (1963).
2. M. S. Dresselhaus, G. Chen, M. Y. Tang, R. Yang, H. Lee, D. Wang, Z. Ren, J. P. Fleurial, and P. Gogna, New directions for low-dimensional thermoelectric materials, *Adv. mater.,* 19(8), 1043-1053 (2007).
3. A. Shakouri, Recent Developments in Semiconductor Thermoelectric Physics and Materials, *Annu. Rev. of Mater. Res.,* 41(1), 399–431 (2011).
4. I. Takeuchi and K. Sandeman, Solid-state cooling with caloric materials, *Phys. Today,* 68(12), 48-54 (2015).
5. A. Ziabari, M. Zebarjadi, D. Vashaee, and A. Shakouri, Nanoscale solid-state cooling: a review, *Rep. Prog. Phys.,* 79(9), 095901 (2016).
6. F. J. DiSalvo, Thermoelectric Cooling and Power Generation, *Science,* 285(5428), 703–706 (1999).
7. M. M. H. Polash, Modeling of Multistage Nernst-Ettingshausen Coolers, *Master's Thesis*, North Carolina State University, Raleigh, NC, 2018.
8. Y. Zheng, T. Lu, Md M. H. Polash, M. Rasoulianboroujeni, N. Liu, M. E. Manley, Y. Deng, P. J. Sun, X. L. Chen, R. P. Hermann, D. Vashaee, J. P. Heremans, and H. Zhao, Paramagnon drag yields a high thermoelectric figure of merit in Li-doped MnTe, *Sci. Adv.*, 5(9), eaat9461 (2019).
9. M. M. H. Polash, F. Mohaddes, M. Rasoulianboroujeni, and D. Vashaee, Magnon-drag thermopower in antiferromagnets versus ferromagnets, *J. Mater. Chem. C*, 8(12), 4049-4057 (2020).
10. M. M. H. Polash and D. Vashaee, Magnon-bipolar carrier drag thermopower in antiferromagnetic/ferromagnetic semiconductors: Theoretical formulation and experimental evidence, *Phys. Rev. B* (2020).
11. M. M. H. Polash, M. Rasoulianboroujeni, and D. Vashaee, Magnon and Spin Transition Contribution in Heat Capacity of Ferromagnetic Cr-doped MnTe: Experimental Evidence for a Paramagnetic Spin-Caloritronic Effect, *Appl. Phys. Lett.*, 117(4), 043903 (2020).
12. H. J. Goldsmid, *The Physics of Thermoelectric Energy Conversion*, San Rafael, CA: Morgan & Claypool Publishers, 2-7–2-8 (2017).

13. A. Miura, H. S. Amin, K. Masuda, H. Tsuchiura, Y. Miura, R. Iguchi, Y. Sakuraba, J. Shiomi, K. Hono, and K.-I. Uchida, Observation of anomalous Ettingshausen effect and large transverse thermoelectric conductivity in permanent magnets, *Appl. Phys. Lett.*, 115, 222403 (2019).
14. K. Behnia, M.-A. Méasson, and Y. Kopelevich, Oscillating Nernst-Ettingshausen Effect in Bismuth across the Quantum Limit, *Phys. Rev. Lett.*, 98, 166602 (2007).
15. R. Modak and K.-I. Uchida, Enhancement of temperature change induced by anomalous Ettingshausen effect in thin Ni films on suspended membrane substrates, *Appl. Phys. Lett.*, 116, 032403 (2020)
16. A. Miura, R. Iguchi, T. Seki, K. Takanashi, and K.-I. Uchida, Spin-mediated charge-to-heat current conversion phenomena in ferromagnetic binary alloys, *Phys. Rev. Mater.*, 4, 034409 (2020).
17. O. Yamashita and S. Tomiyoshi, Effect of geometrical shape on magneto–Peltier and Ettingshausen cooling in Bi and $Bi_{0.88}Sb_{0.12}$ polycrystals, *J. Appl. Phys.*, 92, 3794 (2002)
18. R. Ando and T. Komine, Geometrical contribution to the anomalous Nernst effect in TbFeCo thin films, *AIP Adv.*, 8(5), 056326 (2018).
19. O. Yamashita, K. Satou, and S. Tomiyoshi, Geometrical effect in magneto-Peltier cooling of single crystal Bi, *J. Appl. Phys.*, 95(12), 8233-8239 (2004).
20. S. R. Hawkins, C. F. Kooi, K. F. Cuff, J. L. Weaver, R. B. Horst, and G. M. Enslow, Low-Temperature Ettingshausen Coolers, in *Advances in Cryogenic Engineering, vol 9*, Boston, Springer, 1964, pp. 367-378.
21. S. Sugimoto, Current status and recent topics of rare-earth permanent magnents, *J. Phys. D*, 44(6), 064001, 2011.
22. R. H. Richman and W. P. McNaughton, Permanent-Magnet Materials: Research Directions and Opportunities, *J. Electron. Mater.*, 26(5), 415-422 (1997).
23. A. Nozariasbmarz, H. Collins, K. Dsouza, M. M. H. Polash, M. Hosseini, M. Hyland, J. Liu, A. Malhotra, F. M. Ortiz, F. Mohaddes, V. P. Ramesh, Y. Sargolzaeiaval, N. Snouwaert, M. C. Özturk, and D. Vashaee, Review of wearable thermoelectric energy harvesting: From body temperature to electronic systems, *Appl. Energy*, 258, 114069 (2020).
24. A. Gharleghi, M. M. H. Polash, R. Malekfar , S. Aminorroaya Yamini, and D. Vashaee, Influence of the Order of Fabrication Sequences on the Thermoelectric Properties of Skutterudite CoSb3-Cu0.6Ni0.4 Nanocomposites, *J. Alloys Compd.*, 845, 156188 (2020).
25. J. P. Heremans, Introduction to cryogenic solid state cooling, *Proc. SPIE*, 9821, Tri-Technology Device Refrigeration (TTDR), 98210G (2016).
26. R. Venkatasubramanian, Cascade cryogenic thermoelectric cooler for cryogenic and room temperature applications, *US Patent*, US6505468B2, 2003.
27. S. Karabetoglu, A. Sisman, Z. F. Ozturk, and T. Sahin, Characterization of a thermoelectric generator at low temperatures, *Energy Convers. Manage.*, 62, 47-50 (2012).
28. T. A. Cain, A. P. Kajdos, and S. Stemmer, La-doped SrTiO3 films with large cryogenic thermoelectric power factors, *Appl. Phys. Lett.*, 102, 182101 (2013).
29. C.-J. Hsu, S. M. Sandoval, K. P. Wetzlar, and G. P. Carman, Thermomagnetic conversion efficiencies for ferromagnetic materials, *J. Appl. Phys.*, 110, 123923 (2011).
30. L.-D. Zhao, C. Chang, G. Tan, and M. G. Kanatzidis, SnSe: a remarkable new thermoelectric material, *Energy Environ. Sci.*, 9, 3044-3060 (2016).

31. L-D. Zhao, J. He, D. Berardan, Y. Lin, J.-F. Li, C.-W. Nan, and N. Dragoe, BiCuSeO oxyselenides: new promising thermoelectric materials, *Energy Environ. Sci.*, 7, 2900-2924 (2014).
32. M. Zebarjadi, Thermomagnetic transport in Polycrystalline Samples, *J. Electron. Mater.,* 44(10), 3827-3832 (2015).
33. Marcel Gueltig Frank Wendler Hinnerk Ossmer Makoto Ohtsuka Hiroyuki Miki Toshiyuki Takagi Manfred Kohl, High□Performance Thermomagnetic Generators Based on Heusler Alloy Films, *Adv. Energy Mater.*, 7(5), 1601879 (2017).
34. K. Behnia, M.-A. Measson, and Y. Kopelevich, Nernst Effect in Semimetals: The Effective Mass and the Figure of Merit, *Phys. Rev. Lett.*, 98, 076603 (2007).
35. L. Medici, Thermomagnetic Mechanism for Self-Cooling Cables, *Phys. Rev. Appl.*, 5(2), 024001 (2016).
36. C. F. Kooi, R. B. Horst, and K. F. Cuff, Thermoelectric-Thermomagnetic Energy Converter Staging, *J. Appl. Phys.,* 39(9), 4257-4263 (1968).
37. C. F. Kooi, R. B. Horst, K. F. Cuff, and S. R. Hawkins, Theory of the Longitudinaly Isothermal Ettingshausen Cooler, *J. Appl. Phys.*, 34(6), 1735-1742 (1963).
38. K. Scholz, P. Jandl, U. Birkholz, and Z. M. Dashevskii, Infinite stage Ettingshausen cooling in Bi-Sb alloys, *J. Appl. Phys.,* 75(10), 5406-5408 (1994).
39. K. F. Cuff, R. B. Horst, J. L. Weaver, S. R. Hawkins, C. F. Kooi, and G. M. Enslow, The thermomagnetic figure of merit and Ettingshausen cooling in Bi-Sb alloys, *Appl. Phys. Lett.,* 2(8), 145-146 (1963).
40. T. C. Harman, J. M. Honig, and B. M. Tarmy, Galvano-Thermomagnetic Phenomena. IV. Application to Anisotropic Adiabatic Nernst Generators, *J. Appl. Phys.*, 34(8), 2215-2224 (1963).
41. R. T. Delves, Figure of merit for Ettingshausen cooling, *Br. J. Appl. Phys.*, 15, 105-106 (1964).
42. S. Meyer, Y.-T. Chen, S. Wimmer, M. Althammer, T. Wimmer, R. Schlitz, S. Geprägs, H. Huebl, D. Ködderitzsch, H. Ebert, G. E. W. Bauer, R. Gross, and S. T. B. Goennenwein, Observation of the spin Nernst effect, *Nat. Mater.*, 16, 977–981 (2017).
43. C.-Y. Hou, K. Shtengel, G. Refael, and P. M. Goldbart, Ettingshausen effect due to Majorana modes, *New J. Phys.*, 14, 105005 (2012).
44. S. Ullah and A. T. Dorsey, Critical fluctuations in high-temperature superconductors and the Ettingshausen effect, *Phys. Rev. Lett.*, 65, 2066 (1990).
45. A. Sakai, S. Minami, T. Koretsune, T. Chen, T. Higo, Y. Wang, T. Nomoto, M. Hirayama, S. Miwa, D. Nishio-Hamane, F. Ishii, R. Arita, and S. Nakatsuji, Iron-based binary ferromagnets for transverse thermoelectric conversion, *Nature*, 581, 53–57 (2020).
46. K. Gopinadhan, Y. J. Shin, R. Jalil, T. Venkatesan, A. K. Geim, A. H. Castro Neto, and H. Yang, Extremely large magnetoresistance in few-layer graphene/boron–nitride heterostructures *Nat. Commun.*, 6, 8337 (2015).